

HIGH TEMPERATURE MECHANICAL PROPERTIES OF CVD-SiC THIN FILMS

KWI-IL PARK*, JONG-HO KIM[†], HYUN-KEUN LEE* and DO KYUNG KIM^{*,‡}

**Department of Materials Science and Engineering,
Korea Advanced Institute of Science and Technology (KAIST),
373-1 Gwahangno, Yuseong-gu, Daejeon 305-701, Korea*

*[†]New Metals Research Department,
Research Institute of Industrial Science & Technology (RIST),
32 Hyoja-dong, Nam-gu, Pohang, Gyeongbuk 790-330, Korea*

[‡]dkkim@kaist.ac.kr

Silicon carbide (SiC) coatings were fabricated using a chemical vapor deposition (CVD) process onto a graphite substrate at different deposition temperatures. The mechanical properties such as hardness, modulus, and creep properties from room temperature to 500°C were investigated using nanoindentation techniques. The SiC coatings deposited at 1300°C exhibited a small grain size (0.2 ~ 0.4 μm) and [111] preferred orientation, while the coatings obtained at 1350°C had a large grain size (0.5 ~ 1.0 μm) and [220] preferred orientation. The hardness was decreased with testing temperature, but no significant change in the modulus was measured with testing temperature from high temperature nanoindentation test, and the apparent creep behavior was observed in the high temperature. The high temperature mechanical properties of CVD-SiC coatings were relate to their microstructure and crystal orientation, and CVD-SiC coatings deposited at 1300°C exhibited high stability and reliability at high temperature.

Keywords: SiC coatings; nanoindentation; high temperature mechanical properties; creep, stress exponent.

1. Introduction

Recently, the combinations of MEMS and high temperature operation materials have gained considerable importance due to their significant technological advantages. For examples, shirt-button-sized gas turbines, postage-stamp-sized rockets, and miniature pressure sensors — all devices were designed to operate under the high temperature.^{1,2} Potential materials must possess characteristic properties as chemically inertness and capable of maintaining strength in harsh environments, when exposed to high temperature and high radiation, etc. One such potential material with required characteristic is SiC material.³ SiC film and silicon carbide fiber (SiCf) reinforced silicon carbide composites have gained a great deal of importance in several applications ranging from nuclear power plants for fusion blankets to

[‡]Corresponding author.

functional materials due to their enhanced properties such as high strength, high temperature strength, low electrical conductivity, low thermal decay, low tritium permeability, and resistance to neutron irradiation.^{4–7}

To understand the stability and reliability of SiC coatings on the SiC-MEMS, it is necessary to study their mechanical properties. In the literature, there are several reports on the mechanical properties of the SiC coatings at room temperature (RT),^{3,5,8–10} but higher temperature studies are negligible. Therefore, a detailed investigation on the mechanical properties at higher temperatures is necessary for SiC coatings used in SiC-MEMS operated at harsh environments. In this study, SiC coatings was fabricated by a chemical vapor deposition process at different deposition temperature as 1300 and 1350°C. Scanning electron microscopy, X-ray diffractometer, transmission electron microscopy, and Raman spectroscopy were used to characterize the SiC coatings. Nanoindentation test was performed for the analysis of the hardness, modulus and creep properties up to 500°C.

2. Experiment and Methods

2.1. *Sample preparation and characterization*

Two grades of SiC coatings were fabricated onto graphite substrates were used in this study. A conventional hot-wall type low-pressure chemical vapor deposition technique was used to deposit the SiC coatings. The source gas was methyltrichlorosilane (MTS, CH_3SiCl_3) and the dilution gas (hydrogen). MTS and H_2 were mixed with ratio of 5:1, and the total gas flow rate was fixed at 800 sccm. The pressure in the reaction chamber was maintained as 20 torr, and the deposition time was 1 h. Two deposition temperatures, 1300 and 1350°C were selected to fabricate SiC coatings with different microstructures and crystal orientations.

The phase and crystal orientations were characterized by an X-ray diffractometer (XRD, Rigaku, D/MAX-IIIC X-ray diffractometer, Tokyo, Japan), $\text{CuK}\alpha$ radiation ($\lambda = 0.15406$ nm at 40 kV and 45 mA). The top surface and microstructures of the SiC coatings from each condition were characterized by a scanning electron microscopy (SEM, FE-SEM Philips XL30 FEG, Eindhoven, the Netherlands) and a transmission electron microscopy (TEM, FE-TEM Tecnai G2 F30, FEI Company, Hillsboro, OR). The top surface was obtained as fabricated and a cross-sectional surface was prepared by cutting the specimen. TEM Samples were prepared by precision ion polishing system (PIPS, Gatan Inc. 691, USA). Raman spectroscopy (LabRAM HR UV/Vis/NIR, Horiba Jobin Yvon, France) was performed to provide a more comprehensive phase characterization than XRD, which was unable to detect the excess silicon (Si) or carbon (C) in the SiC coatings.

2.2. *High temperature nanoindentation test*

Chemical vapor deposited (111) and (220) plane orientations SiC coating specimens were used in this study. The uniform top surface of SiC coatings was fabricated by

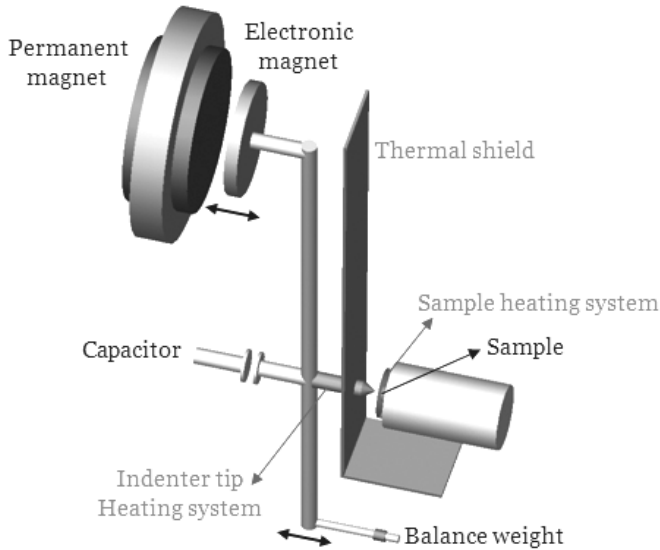


Fig. 1. Schematics of high temperature nanoindentation system.

polishing the specimen, which was fixed onto aluminum holder. Figure 1 shows the schematic illustration of high temperature nanoindentation test performed using a nanoindenter (NanoTest, Micro Materials Ltd., UK) for the analysis of the hardness, modulus and creep properties in the temperature ranging from RT to 500°C. The hardness of each SiC coating specimen was evaluated from 10 indentations, as a function of temperature in step of 100°C from RT to 500°C. The high temperature nanoindentation test was established by thermal drift correction, dual heating systems for temperature match between tip and sample, depth calibration with standard stepped sample. The indentations within each point were spaced 30 μm apart. To make a high temperature hardness indentation, the indenter descends into the sample at a contact loading rate of 1 mN/s. Once the maximum prescribed load is reached, loading stops and the load is held constant for 5 s. Finally, unloading proceeds by removal of the load at a constant rate. Load, depth, and time are recorded continuously during the indentation process. The values of hardness (H) and elastic modulus (E) of the specimens were calculated from load-penetration depth curves.

The nanoindentation creep test was performed as a function of temperature using a commercial nanoindenter. The constant load creep experiments were performed to obtain stress versus strain rate relationships through indentation. Initially, the indenter tip approaches the sample surface and the point at which the indenter contacts the sample surface is marked by a sharp decrease in the descent velocity. Thereafter, the indenter is made to penetrate the sample surface at a specific rate until a predetermined value of the load achieved. This constant load is

maintained for a total duration of 30 s. Subsequently, the sample is unloaded to 20% of the original load value and maintained at the new load for 30 s. This second period is utilized to make corrections for thermal drift. Finally the indenter is withdrawn from the sample surface to terminate the creep experiment. From time-displacement curves at given load, the creep properties can be analyzed and can determine the strain rate and stress exponent.

3. Results and Discussion

3.1. Microstructure

Chemical vapor deposited (111) and (220) plane orientations of SiC coating specimens at different temperature were used in this study. Figures 2(a) and 2(b) show the top surface view and cross-sectional surface of SiC coating specimens deposited at 1300 and 1350°C, respectively. The TEM images of SiC coatings are shown in Figs. 2(c) and 2(d), and X-ray diffraction (XRD) patterns of the corresponding SiC coating specimens are inserted. The SiC coatings deposited at 1300°C exhibited a thin thickness ($\sim 30 \mu\text{m}$), isotropic and domed shape top surface. On the other hand, the SiC coatings obtained at 1350°C had a thick thickness ($\sim 50 \mu\text{m}$), columnar and faceted shape top surface. The SiC coatings used in this study was primarily highly faulted FCC β -SiC. The inserted XRD patterns confirmed the preferred orientation of the SiC coatings deposited at 1300°C as (111) direction

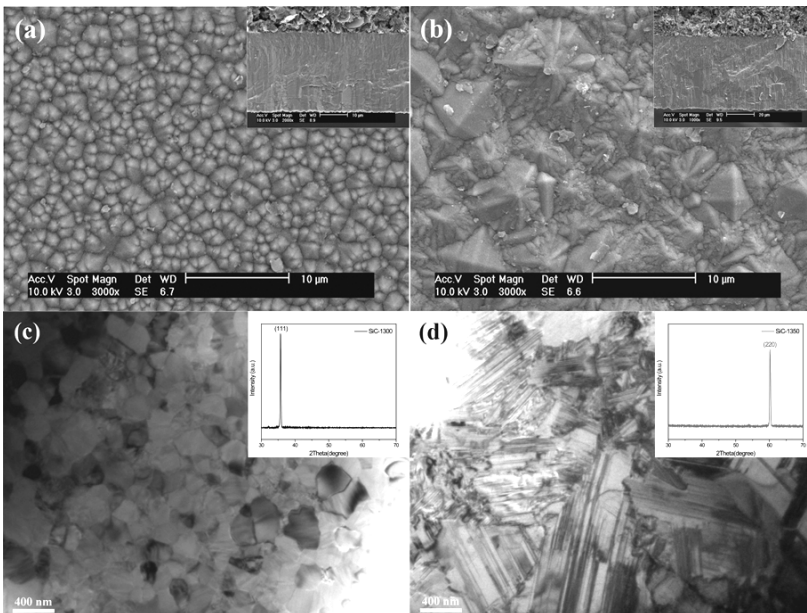


Fig. 2. (a) SEM images, (c) TEM image and XRD pattern of SiC coatings deposited at 1300°C. (b) SEM images, (d) TEM image and XRD pattern of SiC coatings deposited at 1350°C.

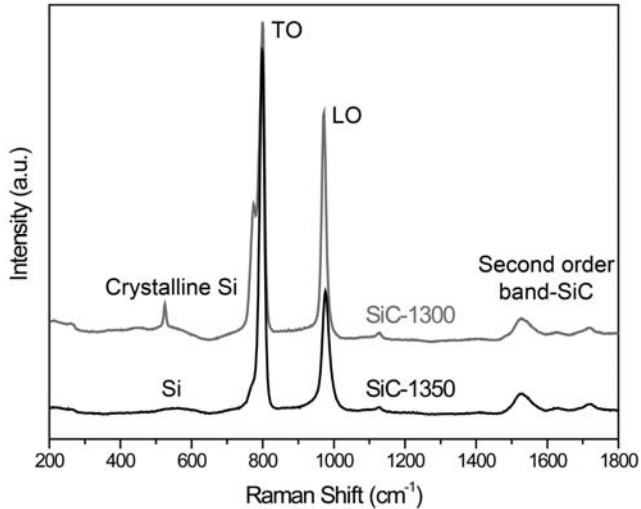


Fig. 3. Raman spectra of SiC coatings obtained at different temperature.

and (220) direction for the specimen fabricated at 1350°C. The effect of deposition temperature on the microstructure of the CVD-SiC are in good agreement with previous studies.^{11,12} TEM images of the SiC coatings deposited at 1300°C exhibited a small grain sizes in the range of 0.2 to 0.4 μm , while the SiC coatings obtained at 1350°C had a large grain sizes in the range of 0.5 to 1.0 μm .

Figure 3 shows the Raman shift of SiC coatings deposited at 1300 and 1350°C. Raman shift confirmed the presence of excess crystalline and amorphous Si for the SiC coatings deposited at different temperatures. In previous study, at temperatures below at 1500°C, Si was co-deposited due to the low surface reactivity of the carbon species participating in the formation of SiC.^{13–15}

3.2. Temperature dependence hardness and elastic modulus of SiC coatings

The typical indentation load-displacement curves obtained at the maximum load as a function of temperature after the high temperature nanoindentation test are shown in Fig. 4. Figures 5(a) and 5(b) show the hardness and modulus data as a function of temperature. In Fig. 4, it is observed that the maximum penetration depth increase with testing temperature and as a result the hardness values shown in Fig. 5(a) are decreased with increasing temperature above 200°C. However, as shown in Fig. 4, the slope of the unloading curve remains unchanged, which reveals that there is insignificant change of modulus as the testing temperature increased. The decrement of the hardness value is largely attributed to the activation of dislocation glide or slip band formation.^{16–19} In case of SiC, the slip at high temperature is dominant and contributes to the hardness decreasing. It is notable that the

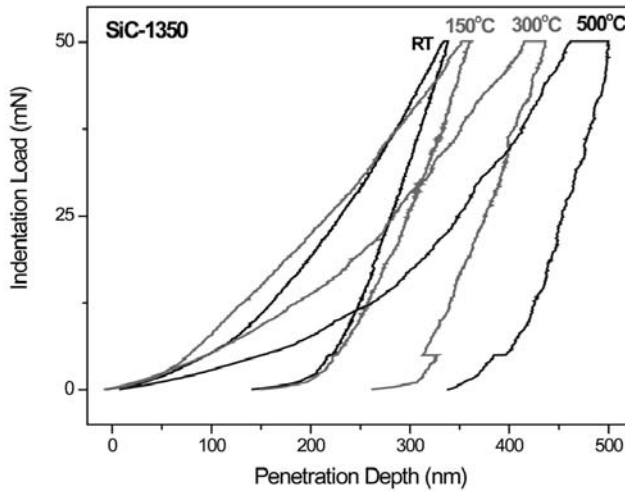


Fig. 4. Nanoindentation Load-Penetration curve at various temperature.

difference in hardness is apparent at RT for the different (111) and (220) planes, while the modulus values shows insignificant difference with different planes, as shown in Fig. 5(b).

3.3. Creep properties of SiC coatings

The significant creep displacement was observed with temperature during the specified hold time. The strain rate and the stress could be applied as the following equations in depth-sensing indentation technique:

$$\dot{\epsilon} \sim \frac{\dot{h}}{h}, \quad \sigma \sim \frac{P}{h^2} \quad (1)$$

where P is the indentation load and h is the instantaneous indenter displacement is calculated by first fit the $h-t$ curve during hold time with the empirical law²⁰:

$$h = h_i + a(t - t_i)^m + kt \quad (2)$$

where h_i , a , m and k are fit constants, and t_i is the time when the creep process is started. Moreover, the stress exponent n , defined as $n = \frac{\partial(\log \dot{\epsilon})}{\partial(\log \sigma)}$, is the slope of the double logarithmic plot of $\dot{\epsilon}$ and σ under isothermal conditions. The fit protocol in Eq. (2) is found to produce very good fit to most of our results, as can be seen from the example (at 500°C) as shown in Fig. 6(a). The corresponding creep strain rate was calculated by Eq. (1) and the double logarithmic plot of strain rate versus stress was obtained from the data in Fig. 6(b).

The slope of the plot strain rate versus stress exhibited the stress exponent and the variation of the stress exponent at different testing temperatures of the SiC coatings are shown in Fig. 7. It can be seen that the stress exponent exhibits

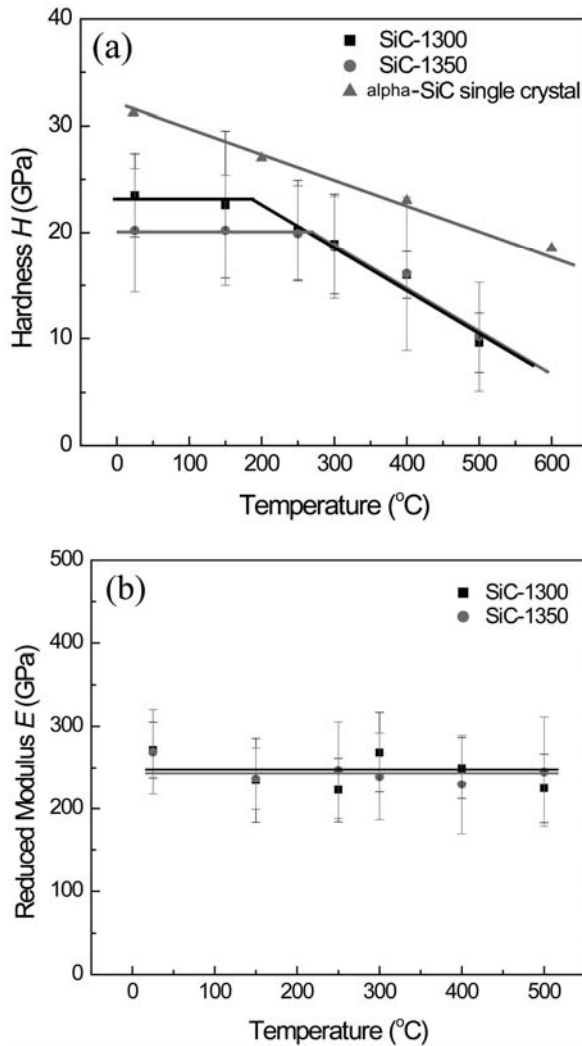


Fig. 5. High temperature nanoindentation results of SiC coatings (a) the hardness plot, (b) the modulus plot.

a strong dependence upon the testing temperature and microstructure of the SiC coatings. The stress exponent values of SiC coatings deposited at 1300 and 1350 $^{\circ}\text{C}$ show continuous decrease of those values down to 10. According to the power law creep, a decrease in stress exponent would result in an increase in creep rate due to a decrease in yield strength.^{21,22} From the significant decrease of stress exponent with the testing temperature, it can be concluded that the creep behaviors is negligible at the lower temperature and apparent creep behaviors observed at high temperature. Even though SiC was widely used as high temperature structural materials due to their a high mechanical strength and thermal resistance, the SiC coatings deposited

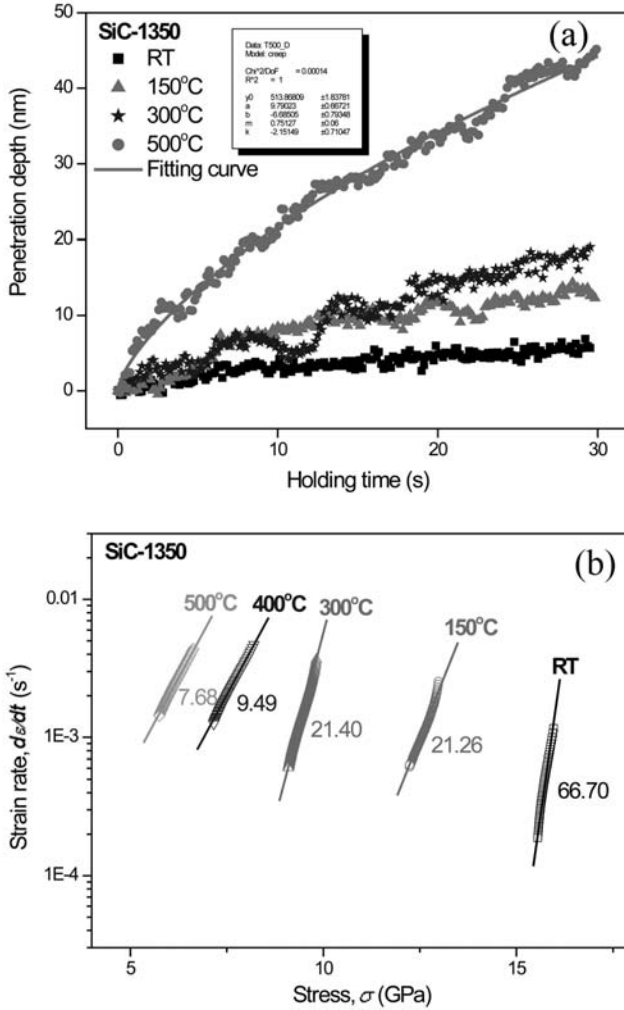


Fig. 6. (a) Experimental and fitting curve for the SiC coatings with holding time at different temperature. (b) Creep curves converted from dwell data of SiC-1350.

at 1300 and 1350°C, used in this study, revealed low creep resistance at 500°C. The SiC coatings produced below 1500°C has excess Si, and it appears that the presence of free Si would serve to seriously degrade creep resistance at elevated temperature. It was observed that the creep rate of SiC exhibited by a large grain size is greater than that of SiC coatings exhibited by a small grain size, and the stress exponent relates to the average grain size of SiC coatings. With decreasing the grain size, the grain boundary area increases and grain boundaries act as more effective barriers to dislocation movement.²³ This explains the reason for SiC coatings deposited at 1300°C exhibits a higher creep resistance.

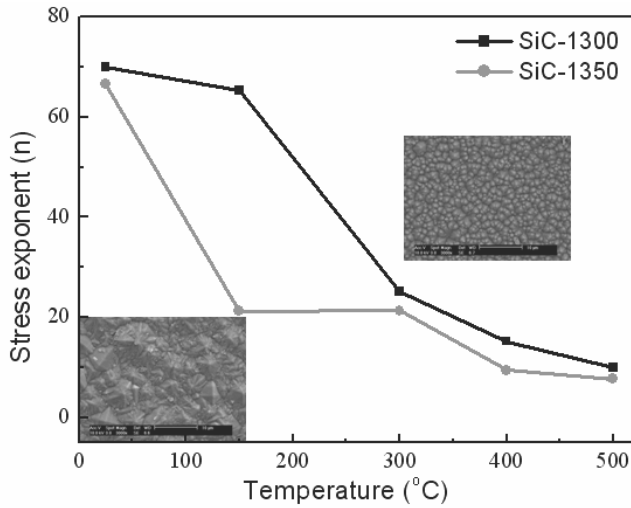


Fig. 7. Plot for stress exponent as a function of indentation temperature for each SiC samples.

4. Conclusions

SiC coatings exhibited the different microstructure and preferred orientation was fabricated by a CVD method at different deposition temperature. The high temperature mechanical properties of the SiC coatings were investigated by nanoindentation test and analyzed the hardness, modulus and creep properties up to 500°C. The SiC coating layers deposited at 1300°C exhibited a small grain size, while the coating layers obtained at 1350°C had a large grain size. The hardness of SiC deposited at different temperature was decreased with testing temperature above 200°C, no significant change in the modulus was observed with testing temperature. SiC coatings showed a small grain size, deposited at 1300°C, exhibits a higher creep resistance. The high temperature mechanical properties of SiC coatings were related to microstructure and SiC coatings deposited at 1300°C showed a small grain size have high stability and reliability at high temperature.

Acknowledgments

This work was supported by Nuclear Research & Development Program of the Korea Science and Engineering Foundation (KOSEF) grant funded by the Korean government (MEST) (Grant No. 2009-0062522).

References

1. S. Nakao, T. Ando and K. Sato, *IEEE, MEMS 2008*, Tucson, AZ, USA, January 13–17 (2008).
2. W. N. Sharpe, G. M. Beheim and O. M. Jadaan, *J. Microelectromech. Syst.* **17** (2008) 244.

3. L. L. Snead, T. Nozawa, Y. Katoh, T. S. Byun and D. A. Petti, *J. Nucl. Mater.* **371** (2007) 329.
4. A. G. Evans, D. R. Mumm and F. S. Pettit, *Prog. Mater. Sci.* **46** (2001) 505.
5. S. G. Hong, T. S. Byun, L. L. Snead and Y. Katoh, *J. Am. Ceram. Soc.* **90** (2007) 184.
6. R. Scholz, *J. Nucl. Mater.* **254** (1998) 74.
7. C. H. Tang, Y. P. Tang, J. H. Li and X. J. Ni, *Nucl. Eng. and Des.* **218** (2002) 91.
8. J. H. Kim, H. K. Lee and D. K. Kim, *Phil. Magazine* **86** (2006) 5383.
9. H. K. Lee and D. K. Kim, *J. Kor. Ceram. Soc.* **44** (2007) 368.
10. T. S. Byun, E. Lara-Curzio, L. L. Snead and Y. Katoh, *J. Nucl. Mater.* **367** (2007) 653.
11. D. J. Kim, D. J. Choi and Y. W. Kim, *Thin Solid Films* **266** (1995) 192.
12. H. S. Kim and D. J. Choi, *Thin Solid Films* **312** (1998) 195.
13. E. Lopez-Honorato, P. J. Meadows, J. Tan and P. Xiao, *J. Mater. Res.* **23** (2008) 1785.
14. R. J. Price and G. R. Hopkins, *J. Nucl. Mater.* **108&109** (1982) 732.
15. B. O. Yavuz and R. E. Tressler, *Ceram. Interl.* **18** (1992) 19.
16. L. J. Vandeperre, F. Giuliani, S. J. Lloyd and W. J. Clegg, *Acta Mater.* **55** (2007) 6307.
17. S. J. Lloyd and W. J. Clegg, *J. Mater. Res.* **16** (2001) 3347.
18. F. Giuliani and W. J. Clegg, *Proc. EMAG' 03*, University of Oxford (2003).
19. V. Domnich, Y. Aratyn, and Y. Gogotsi, *Rev. on Adv. Mater. Sci.* **17** (2008) 33.
20. H. Li and A. H. W. Ngan, *J. Mater. Res.* **19** (2004) 513.
21. G. Cseh, J. Bar, H. J. Gudladt, J. Lendvai and A. Juhasz, *Mater. Sci. Eng. A* **272** (1999) 145.
22. B. Walser and O. D. Sherby, *Scripta Mater.* **16** (1982) 213.
23. R. Roumina, B. Raeisia and R. Mahmudi, *Scripta Mater.* **51** (2004) 497.